Magnetic interactions in the one-dimensional spin-chain metal-organic compounds math xmlns="http://www.w3.org/1998/Math/MathML">mrow>mi>M/mi>msub>mrow>mo>(/mo>msub>mi mathvariant="normal">N/mi>mn>2/mn>/msub>msub>mi mathvariant="normal">H/mi>mn>5/mn>/msub> mo>)/mo>/mrow>mn>2/mn>/msub>msub>mrow>mo>(/mo>msub>mi>SO/mi>mn>4/mn>/msub>mo>)/mo>/mrow>mn>2/mn>/msub>/mrow>/math> math xmlns="http://www.w3.org/1998/Math/MathML">mrow>mo>(/mo>mi>M/mi>mo>=/mo>mi>Cu/mi>mo>,/mo>mo> /mo>mi>Co/mi>mo>,/mo>mo> /mo>mi>Mn/mi>mo>)/mo>/mrow>/math>

S. Calder, L. D. Sanjeewa, V. O. Garlea, J. Xing, R. J. Terry, and J. W. Kolis

Phys. Rev. Materials **6**, 124407 — Published 19 December 2022

DOI: 10.1103/PhysRevMaterials.6.124407

Magnetic interactions in the 1D spin-chain metal-organic compounds $M(N_2H_5)_2(SO_4)_2$ (M=Cu, Co, Mn)

S. Calder,[1,*] L. D. Sanjeewa,[2,3] V. O. Garlea,[1] J. Xing,[4] R. L. Terry,[5] and J. W. Kolis[5]

[1]*Neutron Scattering Division, Oak Ridge National Laboratory, Oak Ridge, Tennessee 37831, USA.*
[2]*University of Missouri Research Reactor (MURR), Columbia, Missouri 65211, USA*
[3]*Department of Chemistry, University of Missouri, Columbia, Missouri 65211, USA*
[4]*Materials Science and Technology Division, Oak Ridge National Laboratory, Oak Ridge, TN 37831.*
[5]*Department of Chemistry and Center for Optical Materials Science and Engineering Technologies, Clemson University, Clemson, South Carolina 29634, USA*

(Dated: October 28, 2022)

Materials with one dimensional (1D) chains of magnetic ions with reduced spin provide a platform for enhanced quantum behavior. Coordination polymers, or equivalently magnetic metal-organic frameworks (MOFs), with both organic and inorganic building blocks offer the ability to design these tailored structural motifs due to the versatility and predictability of organic chemistry. Here we focus on a series of compounds $M(N_2H_5)_2(SO_4)_2$, where M is the transition metal ion Cu^{2+}, Co^{2+} or Mn^{2+}, that forms isolated 1D-spin chains within the bulk crystalline lattice. The behavior of the S=1/2 Cu compound is compared with higher spin Mn and Co based materials through low temperature elastic and inelastic neutron scattering measurements. These provide insights into the magnetic interactions and structure in these materials. In addition, polarized neutron powder diffraction measurements were utilized to determine the site susceptibility tensor in all compounds that provides further insight into the magnetic interactions.

I. INTRODUCTION

Coordination polymers with both organic and inorganic building blocks offer the ability to design and synthesize tailored structural motifs by utilizing the versatility and predictability of organic chemistry[1–5]. Considering current research in condensed matter physics there is a particular focus on reduced dimensionality and reduced spin as promising mechanisms to enhance quantum behavior. Therefore, suitably chosen coordination polymers, or equivalently magnetic metal-organic frameworks (MOFs), can offer promising material design routes to create model systems in which quantum behavior can be investigated. In particular, the tunability of MOFs offers options for magnetic metal ions to be added to well isolated 2D layered and 1D chain coordination structures. The ability to control the spacing of the layers or chains, structural motif and potentially introduce hybrid functionality on the organic linkers affords multiple intriguing research avenues for magnetic coordination polymers in the realm of quantum materials.

One such low dimensional series of materials is the metal hydrazinium sulfates $M(N_2H_5)_2(SO_4)_2$, where M is a transition metal ion. Members of the series were synthesized as early as the 1800's, with the 1D chains being the driving interest in most subsequent studies[6–12]. The crystal structure consists of 1D chains of magnetic ions along the a-axis within a three dimensional crystal structure (see Fig. 1). There is a crossover from 3D to 1D magnetic behavior as a function of temperature and field that points to interesting quantum phenomena in $Cu(N_2H_5)_2(SO_4)_2$[12]. The crystal symmetry of the series $M(N_2H_5)_2(SO_4)_2$ (M=Co, Ni, Zn, Cr and Cu) was investigate in Ref. 13 and shown to all be triclinic, with some small deviations of the lattice constants. The series, therefore, offers a route to compare the effect of altering the magnetic ion and consequently the spin, within a controlled and essentially unaltered low-dimensional environment.

The degree to which the magnetic ions in $M(N_2H_5)_2(SO_4)_2$ can be considered 1D has been considered through various measurements in the literature. Magnetic susceptibility measurements were performed, along with ESR, on $Mn(N_2H_5)_2(SO_4)_2$ to probe the inter and intra-chain interactions[8]. Specific heat studies were undertaken down to 1.5 K[14]. $Fe(N_2H_5)_2(SO_4)_2$ was probed with Mossbauer[9], indicating a 1D regime of AFM interactions preceding a transition to 3D magnetic ordering. These findings are consistent with the broad peak in heat capacity followed by a lambda-like anomaly, consistent with low dimensional behavior. The magnetic susceptibility $M(N_2H_5)_2(SO_4)_2$ (M=Ni, Mn, Fe, Co, Ni, Cu) shows a broad anomaly in the magnetic susceptibility and negative curie Weiss temperatures, indicating AFM 1D chains[7,8].

The magnetic structure has not been experimentally determined in any of the members of $M(N_2H_5)_2(SO_4)_2$ and the exchange interaction energies have only been extracted from bulk measurements of heat capacity and susceptibility. Here, we focus on $M(N_2H_5)_2(SO_4)_2$ (M=Cu^{2+}, Co^{2+}, Mn^{2+}) and perform detailed powder neutron scattering measurements including neutron diffraction, powder neutron polarized diffraction (PNPD) and inelastic neutron scattering. This allows a microscopic picture to be developed of the magnetism in these materials. A consideration when performing neutron scattering on magnetic MOFs that contain hydrogen is the large incoherent scattering from hydrogen. This intro-

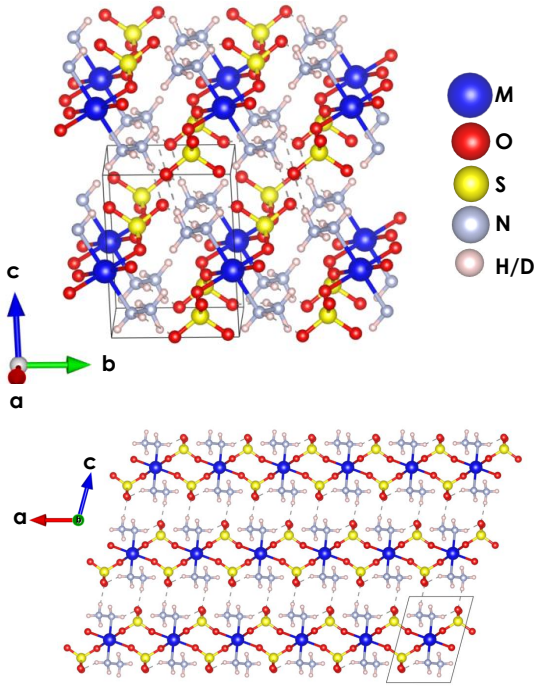

FIG. 1. Crystal structure of $M(N_2H_5)_2(SO_4)_2$ (M = Mn, Co, Cu) with space group $P\bar{1}$ (#2). The unit cell is shown by the solid lines. The magnetic M ions form 1D chains along the a-axis.

duces an increase in the background that can obscure weak signals. We therefore performed deuteration for $Cu(N_2H_5)_2(SO_4)_2$ to produce $Cu(N_2D_5)_2(SO_4)_2$, however we were able to extract magnetic signals in the undeutereated $Mn(N_2H_5)_2(SO_4)_2$. Deuteration routes for $Co(N_2H_5)_2(SO_4)_2$ were not attempted, however as we show the sensitivity of PNPD was leveraged to measure the magnetism. The neutron powder diffraction measurements allowed a determination of the crystal structures to low temperatures, as well as the magnetic structure of $Mn(N_2H_5)_2(SO_4)_2$. An applied field transition was observed in $Mn(N_2H_5)_2(SO_4)_2$ at low fields of 2 T, indicating the ease with which the spins can be tuned. Polarized neutron powder diffraction was used to determined the local magnetic site susceptibilty tensor, which gave insight into the change in anistropy between $Cu(N_2H_5)_2(SO_4)_2$, $Co(N_2H_5)_2(SO_4)_2$ and $Mn(N_2H_5)_2(SO_4)_2$. We note that the increased sensitivity of the half-polarized technique allowed magnetic signals to be observed in all $M(N_2H_5)_2(SO_4)_2$ samples, even those containing hydrogen. Despite not being able to resolve any magnetic Bragg peaks for the $Cu(N_2H_5)_2(SO_4)_2$ inelastic neutron scattering measurements revealed increased inelastic scattering consistent with magnetic excitations at low temperature. A minimal model spin Hamiltonian allowed an estimation of the exchange interactions, with dominant interactions in the 1D chain.

II. METHODS

A. Synthesis

All the reactions were performed using stoichiometric reactions between the transition metal sulfate and the Hydrazine sulfate. Metal sulfate and hydrazine sulfate were dissolved in hot de-ionized water separately. Then the hydrazine sulfate solution was added to the metal sulfate solution while mixing. After mixing the solution for 3-5 minutes, it was cooled down in an ice-bath to afford to precipitate the target product. The precipitate was separated using suction filtrate and washed with de-ionized water and ethanol. Finally, the powder sample was dried at 50 °C for 12 hrs. For $Mn(N_2H_5)_2(SO_4)_2$: $MnSO_4$ $4H_2O$ (2.2306 g) and $N_2H_6SO_4$ (1.302 g); $Co(N_2H_5)_2(SO_4)_2$: $CoSO_4$ $7H_2O$ (2.8111 g) and $N_2H_6SO_4$ (1.302 g); $Cu(N_2H_5)_2(SO_4)_2$: $CuSO_4$ (1.596 g) and $N_2H_6SO_4$ (1.302 g) were used. The deuterated sample of $Cu(N_2D_5)_2(SO_4)_2$was synthesized using anhydrous $CuSO_4$ and $N_2D_6SO_4$. Herein, both chemicals were dissolved in D_2O and the final product was washed by using deuterated ethanol. The sample purity of the powder sample were checked using powder x-ray diffraction, PANalytical XPert Pro MPD diffractometer with Cu K1 radiation (λ = 1.5418 Å).

B. Magnetic property characterization

Temperature-dependent and field dependent magnetic susceptibility measurements were performed using a Quantum Design Magnetic Property Measurement System (MPMS). Powder samples were pressed into a 1/8 inch pellet and affixed to a quartz rod using GE varnish. The total mass of the samples were 8-10 mg. The temperature dependent magnetization measurements were carried out using these pellets from 2 to 350 K in an applied magnetic field of up to 50 kOe. Additionally, isothermal magnetization measurements were performed between 2-100 K up to a 60 kOe magnetic field. The heat capacity (Cp) of the sample was measured using a Physical Property Measurement System (PPMS) between 2-50 K under 0 and 110 kOe applied magnetic fields. Heat capacity of the $Cu(N_2D_5)_2(SO_4)_2$ was measured down to 0.4 K.

C. Neutron powder diffraction

Neutron powder diffraction measurements were carried out on the HB-2A powder diffractometer at the High Flux Isotope Reactor (HFIR), Oak Ridge National Laboratory (ORNL)[15,16]. Hydrogen based materials present an extra challenge for neutron scattering by both adding to the neutron absorption and creating an increased background from incoherent scattering. These effects can be easier to account for with constant wavelength instruments due to the simpler data correction. A germanium

monochromator was used to select a wavelength of 2.41 Å from the Ge(113) reflection and 1.54 Å from the Ge(115) reflection. The pre-mono, pre-sample and pre-detector collimation was open-21'-12'. A pyrolytic graphite (PG) filter was placed before the sample to remove higher order reflections for the 2.41 Å wavelength. The samples were contained in a 6 mm diameter vanadium can and cooled in a liquid ^{4}He cryostat with an in-situ 3-sample changer stick in the temperature range 1.5 K - 300 K. The $Cu(N_2D_5)_2(SO_4)_2$ and $Co(N_2H_5)_2(SO_4)_2$ samples were also measured to 0.3 K in a ultra-low temperature multi-sample changer that can hold up to six samples. For these measurements the samples were loaded in Al cans with an overpressure of helium exchange gas of 10 atm. to facilitate cooling of the powder to base temperature. The diffraction pattern was collected by scanning a 120° bank of 44 ^{3}He detectors in 0.05° steps to give 2θ coverage from 5° to 130°. Rietveld refinements were performed with Fullprof[17]. Symmetry allowed magnetic structures were considered using both representational analysis with SARAh[18] and magnetic space groups with the Bilbao Crystallographic Server[19].

D. Polarized neutron powder diffraction

Polarized neutron powder diffraction (PNPD) was performed on the HB-2A powder diffractometer using the 2.41 Å wavelength[16]. A supermirror V-cavity was placed in the incident beam to select and transmit one polarization state. A guide field "flipper" after the V-cavity allows the polarization state of the beam to be controlled between spin-up and spin-down states. The sample, in pressed pellet form, was contained within a vertical field asymmetric cryomagnet. It has been shown in Refs. 20 and 21 that the local site susceptibility tensor can be determined from measurements of a sample in an applied field in the linear M/H regime by taking the difference of diffraction patterns measured with an incident beam with spin-up and then spin-down. Such measurements were taken on $M(N_2H_5)_2(SO_4)_2$ (M=Cu, Co, Mn) above any magnetic long range ordering in applied fields of 2.5 T - 3 T. This is satisfied for a wide temperature and field range in all the samples, as we show in magnetization measurements.

E. Inelastic neutron scattering

Inelastic neutron scattering (INS) measurements were performed on the time-of-flight direct geometry Hybrid Spectrometer (HYSPEC) at the Spallation Neutron Source (SNS). Measurements were taken at 0.3 K, 3 K and 10 K using a ^{3}He insert in a ^{4}He cryostat. An incident energy of E_i=3.8 meV was select with a 360 Hz Fermi chopper giving a resolution of 0.09meV at the elastic line. Analysis of the magnet excitations was performed with linear spin wave theory using SpinW[22].

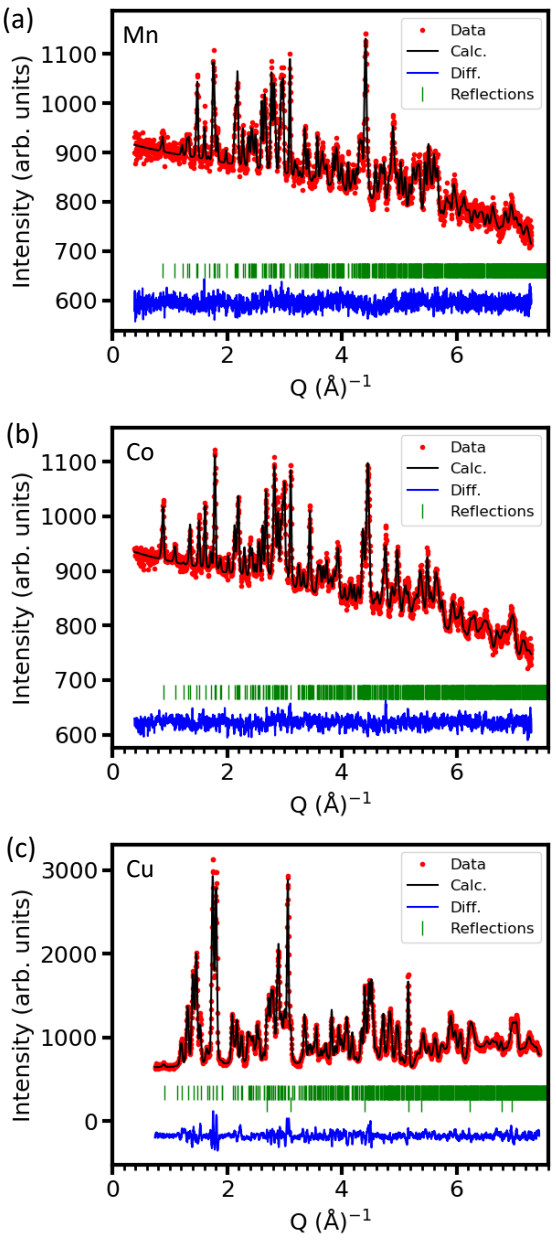

FIG. 2. Refinement of neutron powder diffraction data taken on the HB-2A diffractometer for (a) $Mn(N_2H_5)_2(SO_4)_2$ at 20 K, (b) $Co(N_2H_5)_2(SO_4)_2$ at 1.5 K and (c) $Cu(N_2D_5)_2(SO_4)_2$ at 0.3 K. The lower tick marks in the $Cu(N_2D_5)_2(SO_4)_2$ refinement correspond to reflections from the Al sample holder.

III. RESULTS AND DISCUSSION

A. Crystal structure of $M(N_2H_5)_2(SO_4)_2$

We began with probing the crystal structure of $Mn(N_2H_5)_2(SO_4)_2$, $Co(N_2H_5)_2(SO_4)_2$ and $Cu(N_2D_5)_2(SO_4)_2$ with neutron powder diffraction, see Fig. 2(a)-(c). For

TABLE I. Refined crystal structure parameters for $Mn(N_2H_5)_2(SO_4)_2$ at 20 K for space group $P\bar{1}$ (#2) with lattice constants a=5.395(51)Å, b=5.858(6)Å, c=7.399(7)Å, α=92.67(5)°, β=104.38(4)°, γ=99.21(5)°.

Atom	x	y	z	site
Mn	0.5	0	0.5	$1f$
S	0.136(4)	0.255(4)	0.711(3)	$2i$
O	0.127(2)	0.774(2)	0.406(1)	$2i$
O	0.339(2)	0.277(2)	0.602(2)	$2i$
O	0.164(3)	0.047(2)	0.831(1)	$2i$
O	0.811(2)	0.535(2)	0.152(2)	$2i$
N	0.435(2)	0.188(1)	0.231(1)	$2i$
H	0.371(3)	0.068(3)	0.120(2)	$2i$
H	0.606(4)	0.280(4)	0.236(3)	$2i$
N	0.233(1)	0.329(1)	0.215(1)	$2i$
H	0.208(5)	0.393(4)	0.087(3)	$2i$
H	0.072(4)	0.231(3)	0.221(2)	$2i$
H	0.300(5)	0.444(5)	0.330(4)	$2i$

TABLE II. Refined crystal structure parameters for $Co(N_2H_5)_2(SO_4)_2$ at 1.5 K for space group $P\bar{1}$ (#2) with lattice constants a=5.311(4)Å, b=5.807(4)Å, c=7.324(5)Å, α=91.84(5)°, β=105.65(4)°, γ=98.82(5)°.

Atom	x	y	z	site
Co	0.5	0	0.5	$1f$
S	0.148(4)	0.245(3)	0.713(3)	$2i$
O	0.136(2)	0.778(2)	0.406(1)	$2i$
O	0.342(2)	0.271(2)	0.600(1)	$2i$
O	0.153(2)	0.042(2)	0.834(1)	$2i$
O	0.798(2)	0.534(2)	0.156(1)	$2i$
N	0.431(1)	0.177(2)	0.240(1)	$2i$
H	0.380(3)	0.068(3)	0.130(2)	$2i$
H	0.615(3)	0.283(2)	0.230(2)	$2i$
N	0.242(1)	0.328(1)	0.218(1)	$2i$
H	0.243(3)	0.406(3)	0.095(2)	$2i$
H	0.082(3)	0.232(2)	0.223(2)	$2i$
H	0.322(3)	0.466(2)	0.339(2)	$2i$

$Mn(N_2H_5)_2(SO_4)_2$ and $Co(N_2H_5)_2(SO_4)_2$ the increased background and Q dependence from hydrogen is evident, however the structural Bragg peaks are clearly resolved above this background. The effectiveness of deuteration is evident in $Cu(N_2D_5)_2(SO_4)_2$ through the observation of a decreased and flat background.

Refinements for $Cu(N_2D_5)_2(SO_4)_2$, $Mn(N_2H_5)_2(SO_4)_2$ and $Co(N_2H_5)_2(SO_4)_2$ are shown in Fig. 2 and the refined parameters are in Tables I, II and III. Due to the large number of variables the thermal parameters were fixed in the refinements. All compositions were fit with the low symmetry triclinic $P\bar{1}$ (#2) space group, consistent with previous reports in the literature[13,23]. In this centrosymmetric structure the metal ion is coordinated by four oxygen ions from four different SO_4 groups and by two N_2H_5, together forming a distorted octahedral coordination. The 1D-chains are formed by the SO_4 group bridging between two adjacent metal ions, see Fig. 1. This system has a linear 1D-chain along the direction of the $SO_4{}^{2-}$ bridging linkers. The

TABLE III. Refined crystal structure parameters for $Cu(N_2D_5)_2(SO_4)_2$ at 0.3 K for space group $P\bar{1}$ (#2) with lattice constants a=5.394(4)Å, b=5.647(4)Å, c=7.142(5)Å, α=90.54(4)°, β=104.31(6)°, γ=97.20(4)°.

Atom	x	y	z	site
Cu	0.5	0	0.5	$1f$
S	0.177(3)	0.257(3)	0.732(2)	$2i$
O	0.096(2)	0.758(2)	0.419(2)	$2i$
O	0.363(2)	0.267(2)	0.616(2)	$2i$
O	0.173(2)	0.037(1)	0.849(1)	$2i$
O	0.809(2)	0.539(2)	0.153(1)	$2i$
N	0.432(1)	0.170(1)	0.252(1)	$2i$
D	0.387(2)	0.057(2)	0.125(2)	$2i$
D	0.611(2)	0.290(2)	0.238(1)	$2i$
N	0.220(1)	0.330(1)	0.227(1)	$2i$
D	0.222(3)	0.420(2)	0.099(1)	$2i$
D	0.054(2)	0.205(2)	0.213(1)	$2i$
D	0.288(3)	0.429(2)	0.355(2)	$2i$

distance between the magnetic ions in the chains is ∼5.4 Å, precluding direct exchange, instead requiring superexchange through $M-O-S-O-M$. The interchain distance is only slightly larger at ∼5.8 Å, however they are linked by weaker van der Waals bonding between the terminal N_2H_5 and SO_4 groups which is expected to lead to weaker magnetic interactions. The further metal-metal distance along the c-axis is appreciably larger at 7.4 Å. Consequently the magnetic interactions in the 1D chains along the a-axis are expected to be significantly larger than those between the chains. This was supported by the early analysis in the literature[8].

B. Magnetic ordering in $M(N_2H_5)_2(SO_4)_2$

1. $Mn(N_2H_5)_2(SO_4)_2$

$Mn(N_2H_5)_2(SO_4)_2$ has the largest spin per magnetic site and so is the starting point for considering the magnetism. Fitting the magnetic susceptibility to the Curie-Weiss law gives an effective moment of $6\mu_B$/Mn ion with a Weiss constant of -13 K, indicative of antiferromagnetic interactions, as shown in Fig. 3(a). The zero field heat capacity has a broad feature that develops below 10 K with a sharp anomaly around 2 K (Fig. 3(d)). There is a corresponding anomaly in the magnetization at 2 K. This behavior is indicative of the development of short-range correlations before a transition to long range magnetic ordering.

Comparing neutron powder diffraction measurements of $Mn(N_2H_5)_2(SO_4)_2$ at 1.5 K and 20 K shows the development of additional reflections that indicate long-range magnetic order, see Fig. 4. Measuring the temperature dependence of the intensity of the strongest Bragg reflection at Q=0.65Å^{-1} shows a sharp on-set of intensity and fitting this to a power law indicates a transition around 2.4(3) K. This is consistent with the temperature of the sharp anomaly in the heat capacity of

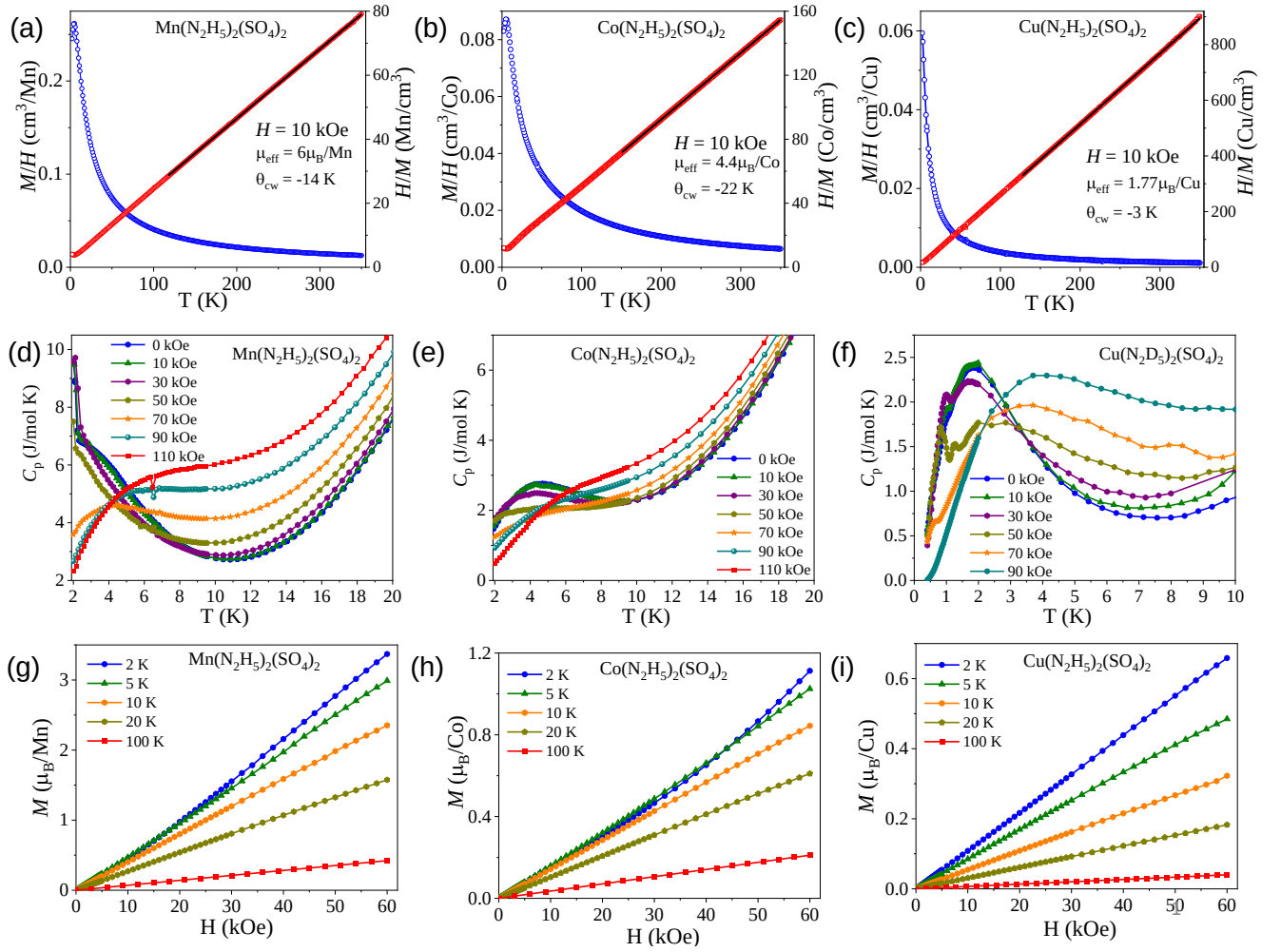

FIG. 3. Magnetization measurements for (a) $Mn(N_2H_5)_2(SO_4)_2$, (b) $Co(N_2H_5)_2(SO_4)_2$ and (c) $Cu(N_2D_5)_2(SO_4)_2$. The solid line is a fit to the Curie-Wiess law, with values used for $\mu_{\rm eff}$ and θ_W shown. Heat capacity measurements for (d) $Mn(N_2H_5)_2(SO_4)_2$, (e) $Co(N_2H_5)_2(SO_4)_2$ and (f) $Cu(N_2D_5)_2(SO_4)_2$ under various applied fields. All samples show a broad feature at low temperature, indicative of low dimensional correlations. M/H measurements at select temperatures for (g) $Mn(N_2H_5)_2(SO_4)_2$, (h) $Co(N_2H_5)_2(SO_4)_2$ and (i) $Cu(N_2D_5)_2(SO_4)_2$.

$Mn(N_2H_5)_2(SO_4)_2$ around 2K in Fig. 3(d). The magnetic reflections can be indexed to a k=(0.5,0,0.5) propagation vector. There is only one allowed magnetic space group $P_s\bar{1}$ (#2.7) based on this propagation vector and paramagnetic space group. The magnetic moment direction is not constrained within this magnetic space group, with symmetry allowed moments along the a, b and c-axis. Before refining the data to determine the spin direction, a consideration of the propagation vector k=(0.5,0,0.5) and peak intensities indicates spins primarily along the b-axis and antiferromagnetic ordering along the a and c-axis to give the required magnetic cell doubling in those directions. Refinement of the data gives the magnetic structure shown in Fig. 4(d), where the spins form AFM 1D-chains along the a-axis with an ordered moment size of 3.2(1) $\mu_{\rm B}$/Mn ion. Refinements indicate that the m_a and m_c components are almost null within the measurement uncertainty.

To further probe the magnetic order with neutron diffraction in $Mn(N_2H_5)_2(SO_4)_2$ a magnetic field up to 5.5 T was applied at 1.5 K. As shown in Fig. 4(e)-(f) the intensity of the (001) reflection increases while (0.5,0,-0.5) intensity decreases, with a crossover above 2 T. This is consistent with a change from AFM to spin polarized FM ordering in the paramagnetic regime under applied magnetic field.

2. $Co(N_2H_5)_2(SO_4)_2$

The high temperature magnetic susceptibility for $Co(N_2H_5)_2(SO_4)_2$ follows Curie-Weiss behavior, with an effective moment of 4.5$\mu_{\rm B}$/Co ion and a large negative Weiss temperature of -29K. For $Co(N_2H_5)_2(SO_4)_2$ there

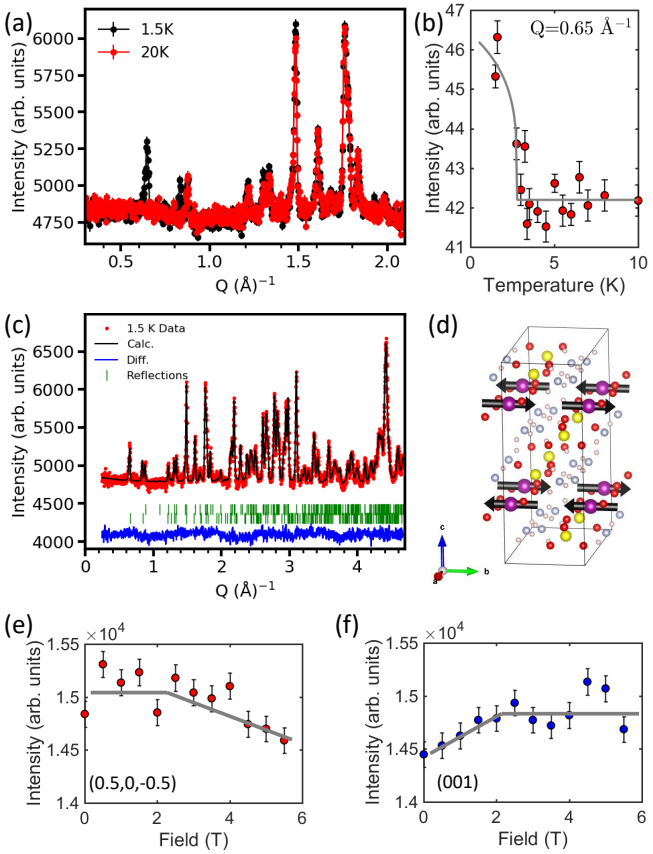

FIG. 4. (a) Neutron diffraction measurements on $Mn(N_2H_5)_2(SO_4)_2$ at 1.5 K and 20 K. (b) Intensity at Q=0.65Å^{-1} from 1.5 K to 10 K. The solid line is a fit to a power law. (c) Refinement of the crystal and magnetic structure at 1.5 K. (d) Magnetic structure with spins represented as arrows. Change in intensity with applied magnetic field for the (e) (0.5,0,-0.5) and (f) (001) reflections. The line is a guide to the eye indicating a field induced transition H_c>2 T.

is an indication of a downturn in the M/H curve, Fig. 3(b), however the heat capacity does not show any corresponding sharp anomaly above 2 K. Instead there is just a broad feature that would indicate short-range correlations. The larger Weiss temperature and suppressed ordering temperature compared to $Mn(N_2H_5)_2(SO_4)_2$ potentially places $Co(N_2H_5)_2(SO_4)_2$ closer to the ideal 1D limit.

The effective magnetic moment of Co^{2+} is normally higher than the spin only value of Co^{2+} with S = 3/2, (i.e. $\mu_{\rm eff}$ = 3.8 $\mu_{\rm B}$). This could be due to the significant orbital contribution since orbital moments are unquenched for Co^{2+} in octahedral environment ($t_{2g}^5 e_g^2$, S = 3/2, L = 3). However, it is important to highlight that at lower temperatures the ground state of a distorted octahedral Co^{2+} is a Kramers doublet. Therefore, at lower temperatures the magnetic properties of Co^{2+} is determined by the lowest Kramers doublet, $J_{\rm eff} = \frac{1}{2}$. The effective spin-1/2 ground state at lower temperatures has been reported in many Co^{2+}-triangular magnetic materials. The spin-state of $Co(N_2H_5)_2(SO_4)_2$ was considered in the literature and proposed to be $J_{\rm eff} = \frac{1}{2}$ based on specific heat results and crystal field arguments[8,14]. The presence of such a state in Co^{2+} can be confirmed by measuring crystal field excitations using high-energy inelastic neutron scattering.[24–26].

From neutron powder diffraction measurements carried out down to 0.3 K, no long range magnetic ordering was observed. We stress this lack of ordering could readily be explained by the background scattering from hydrogen obscuring the magnetic reflections. We discuss polarized measurements in section III C, however it will be of interest to explore routes to deuterate the material to further investigate any low temperature ordering.

3. *$Cu(N_2D_5)_2(SO_4)_2$*

We now turn to the S=1/2 $Cu(N_2H_5)_2(SO_4)_2$, for which a magnetic phase diagram was proposed in the literature based on magnetic susceptibility and specific heat measurements[12]. This indicated 1D ordering developing below 2 K with long range antiferromagnetic order below 1 K, in zero field. We synthesized a deuterated sample, $Cu(N_2D_5)_2(SO_4)_2$, and performed similar magnetic susceptibility and specific heat measurements, see Fig. 3(c),(f). The behavior of $Cu(N_2D_5)_2(SO_4)_2$ is consistent with $Cu(N_2H_5)_2(SO_4)_2$, with a broad feature centered around 2 K in the heat capacity suggesting 1D correlations and then a sharp anomaly below 1 K indicating long range ordering.

To uncover any long range ordering we performed neutron powder diffraction down to 0.3 K, however, no additional magnetic scattering was observed in the diffraction data. Given the small S=1/2 moment and potential for quantum fluctuations in this low dimensional material the lack of any signal is not direct evidence of no long range magnetic ordering. We investigate this further with both PNPD and inelastic neutron scattering.

4. *Phase diagrams for $M(N_2H_5)_2(SO_4)_2$*

Magnetic phase digrams for $M(N_2H_5)_2(SO_4)_2$ are shown in Fig. 5(a)-(c). These are determined based on anomalies in the heat capacity, susceptibility and neutron scattering data that indicate magnetic phase transitons. The broad curves in the heat capacity are indicative of short range order and the sharper features indicate long range ordering. The phase diagram for $Cu(N_2D_5)_2(SO_4)_2$, Fig. 5, is consistent with that reported for $Cu(N_2H_5)_2(SO_4)_2$ in Ref. 12, indicating that the deuteration does not impact the magnetism. For $Mn(N_2H_5)_2(SO_4)_2$ and $Cu(N_2D_5)_2(SO_4)_2$ regions of long-range order are reported based on the position of the sharp anomaly in the heat capacity. We stress that from neutron scattering long range order was only observed in $Mn(N_2H_5)_2(SO_4)_2$ and not $Cu(N_2D_5)_2(SO_4)_2$.

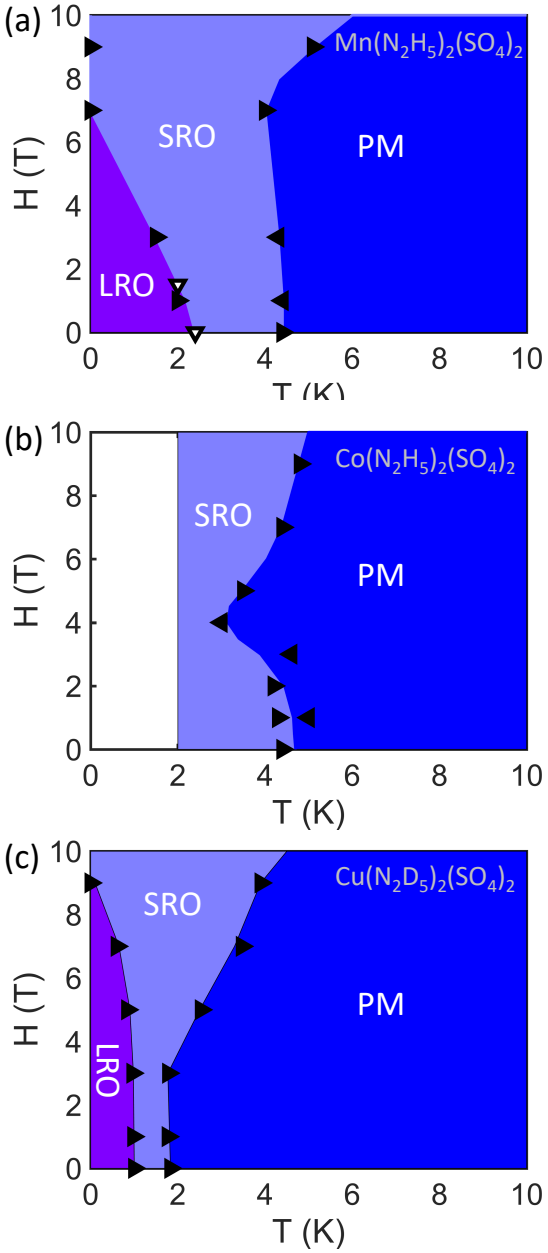

FIG. 5. Phase diagram for (a) $Mn(N_2H_5)_2(SO_4)_2$, (b) CoHSON, (c) $Cu(N_2D_5)_2(SO_4)_2$. The regions of long range order (LRO), short range order (SRO) and paramagnetism (PM) are shown, as determined from heat capacity (right triangles), magnetic susceptibility (left triangles) and neutron diffraction (down triangles with white filling).

For the case of $Co(N_2H_5)_2(SO_4)_2$ heat capacity and magnetic susceptbility was only measured to 2 K. The heat capacity for $Co(N_2H_5)_2(SO_4)_2$showed no sharp anomaly, just a broad peak indicative of short range order. The low temperature neutron scattering data from 0.3 K - 2 K for $Co(N_2H_5)_2(SO_4)_2$observed no ordering, however since we cannot rule out a weak signal being beyond the limits of the measurement no phase diagram is reported below 2 K for $Co(N_2H_5)_2(SO_4)_2$.

C. Local site susceptibility tensor with Polarized Neutron powder diffraction

We extended our neutron powder diffraction measurements by performing PNPD to determine the atomic site susceptibility tensor of the magnetic ions. This can be done in a neutron diffraction experiment by measuring the change in the intensity of the diffraction pattern for a sample in an applied magnetic field as the incident neutron polarization state is either parallel (I_+) or anti-parallel (I_-) to the applied field direction. The technique is described in detail in Refs. 20 and 21. The flipping difference method is used here, with the intensity difference given by:

$$I_+ - I_- \propto 2\Re[F_N^\star \langle \mathbf{F}_{M,\perp} \cdot \mathbf{P} \rangle], \tag{1}$$

where F_N and $\mathbf{F}_M$ are the nuclear and magnetic structure factors and $\mathbf{P}$ is the polarization value of the incident beam. Angular brackets account for the powder averaging. This relationship reveals that the difference signal is only observed in PNPD when there is a magnetic signal and also that the signal is enhanced at larger nuclear reflections.

The magnetic structure factor is given by $\mathbf{F}_M(Q) = \sum_i \mathbf{m_i} f_m(Q) \exp(iQ.r_i)$, where the sum is over the unit cell, $f_m(Q)$ is the magnetic form factor and $\mathbf{m_i}$ is the magnetic moment on atom i. $\mathbf{m_i}$ in a magnetic field satisfies the behavior:

$$\bar{\chi_i} = \frac{\mathbf{B}}{\mathbf{m_i}} = \begin{pmatrix} \chi_{11} & \chi_{12} & \chi_{13} \\ \chi_{12} & \chi_{22} & \chi_{23} \\ \chi_{13} & \chi_{23} & \chi_{33} \end{pmatrix}, \tag{2}$$

The site symmetry determines the allowed non-zero tensor components. The CrysPy software was utilized to refine the PNPD data and extract $\bar{\chi_i}$.[21]

For the above PNPD discussion to be valid the sample should have a net moment and be in the linear M/H region, which is satisfied for a large phase space of $Mn(N_2H_5)_2(SO_4)_2$, $Co(N_2H_5)_2(SO_4)_2$ and $Cu(N_2D_5)_2(SO_4)_2$ in Fig. 3(g)-(i). The PNPD methodology can therefore provide insights into materials beyond traditional neutron diffraction and the measurement is highly sensitive to even weak magnetic signals below $0.1\mu_B$. Consequently, as we will show, we were able to extract magnetic signals for all three $M(N_2H_5)_2(SO_4)_2$ materials. Due to the number of variables we found that refining the PNPD data using more than the transiton metal ions did not produce an improved fit. However, the extended nature of the bonds make it of interest to consider the extension of the magnetization in general in magnetic MOFs using PNPD to the anions.

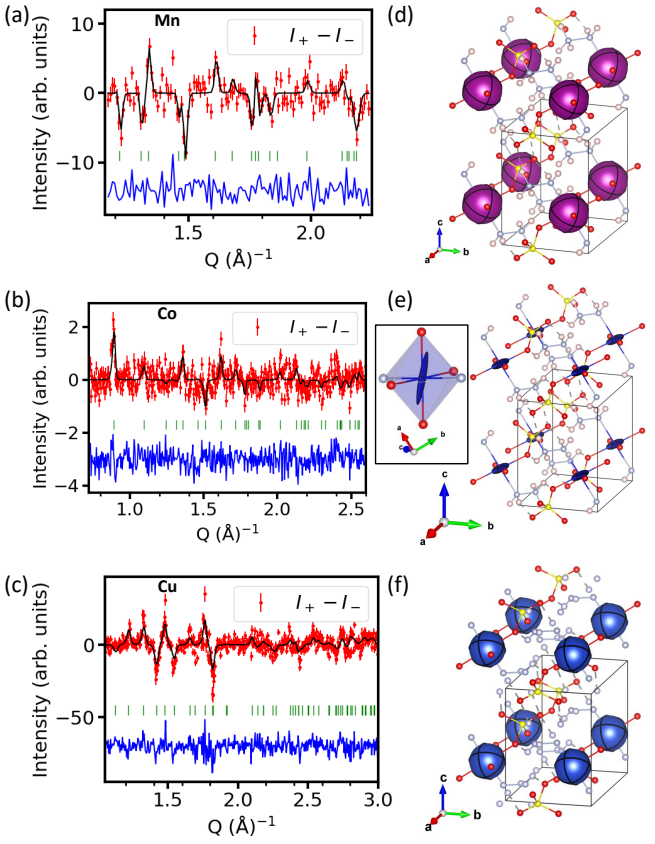

FIG. 6. Polarized neutron powder diffraction measurements on the HB-2A diffractometer. Difference measurements of $I_+ - I_-$ for (a) $Mn(N_2H_5)_2(SO_4)_2$, (b) $Co(N_2H_5)_2(SO_4)_2$ and (c) $Cu(N_2D_5)_2(SO_4)_2$ and refined fit using a site susceptibility model. The magnetization ellipsoid representation of the local site susceptibility for the (d) Mn ion, (e) Co ion and (f) Cu ion.

1. $Mn(N_2H_5)_2(SO_4)_2$

As shown with unpolarized neutron diffraction $Mn(N_2H_5)_2(SO_4)_2$ hosts long range magnetic order below 2 K (Fig. 4). We therefore performed the PNPD measurements above the transition at 5 K and 2.5 T, in the paramagnetic regime (see phase diagram in Fig. 5). As shown in Fig. 3(g) this is in the required linear M/H region. The difference of spin up and spin down $(I_+ - I_-)$ incident polarized neutrons is shown in Fig. 6(a). The low symmetry of the magnetic ion in $M(N_2H_5)_2(SO_4)_2$ results in all six χ terms being allowed (3 diagonal and 3 off-diagonal). However, there was a strong correlation between the terms and identical results were obtained using an isotropic susceptibility tensor compared to using all the variables in the full matrix tensor. Consequently we proceed with an isotropic model and the best fit to the data using the CrysPy software is shown in Fig. 6(a). The eigenvalues of the susceptibility tensor are the diagonal values of 0.25 $\mu_B T^{-1}$. The corresponding isotropic magnetization ellipsoid can be visualized in Fig. 6(d). This is consistent with Heisenberg spins, which is indeed predicted for the Mn ion[14] and provides an experimental verification from powder data.

The magnetization tensor, equation 2, for Mn in $Mn(N_2H_5)_2(SO_4)_2$ obtained from refinement of the PNPD data constrained to isotropic terms was found to be

$$\chi_{\mathrm{Mn}} = \begin{pmatrix} 0.25(3) & 0 & 0 \\ 0 & 0.25(3) & 0 \\ 0 & 0 & 0.25(3) \end{pmatrix} \mu_B T^{-1}$$

2. $Co(N_2H_5)_2(SO_4)_2$

$Co(N_2H_5)_2(SO_4)_2$ was measured with PNPD under a 3 T applied field at 8 K, in the linear M/H region of Fig. 3(h). Also see the phase diagram shown in Fig. 5 confirming this is the paramagnetic region. Despite not observing any long range order with unpolarized neutrons several reflections showed a change in intensity for spin-up and spin-down polarized measurements, as shown in Fig. 6(b). The difference data was modeled by refining the susceptibility values, no strong covariance was found when utilizing the full symmetry determined anisotropy susceptibility parameters. The magnetization tensor, equation 2, for Co in $Co(N_2H_5)_2(SO_4)_2$ obtained from refinement of the PNPD data was found to be

$$\chi_{\mathrm{Co}} = \begin{pmatrix} 0.183(28) & 0.135(20) & -0.067(58) \\ 0.135(20) & 0.0999(65) & 0.015(28) \\ -0.067(58) & 0.015(28) & 0.068(31) \end{pmatrix} \mu_B T^{-1}$$

Diagonalizing this tensor gives eignevalues $0.029\mu_B T^{-1}$, $0.088\mu_B T^{-1}$, $0.291\mu_B T^{-1}$. This reveals anisotropic behavior indicating the Co spins are Ising-like. The magnetization ellipsoid can be visualized in Fig. 6(e) and shows the magnetization is largely confined to the a-b plane and follows the local Co-O bond direction. The observation of anisotropic magnetism adds to the previous reports in the literature that suggested either XY or Ising linear chain models to be appropriate for $Co(N_2H_5)_2(SO_4)_2$.[8,14]

3. $Cu(N_2D_5)_2(SO_4)_2$

Similar PNPD measurements were performed for $Cu(N_2D_5)_2(SO_4)_2$, this time without the added background from hydrogen due to the deuteration. Despite no diffraction signal being present with non-polarized powder diffraction, well resolved scattering was observed in the PNPD measurements for spin-up and spin-down $(I_+ - I_-)$ incident polarized neutrons, shown in Fig. 6(c). These measurements were taken at 5 K and a field of 2.5 T, within the linear M/H paramagnetic regime, as shown in Fig. 5. The initial refinement was performed

with all the χ terms as variables, as determined by the site symmetry. This produced values of zero within error for off-diagonal terms and closely related diagonal terms. Consequently, as was done for the $Mn(N_2H_5)_2(SO_4)_2$, we limit the analysis to an isotropic susceptibility tensor and found the best fit to be

$$\chi_{\mathrm{Cu}} = \begin{pmatrix} 0.0364(36) & 0 & 0 \\ 0 & 0.0364(36) & 0 \\ 0 & 0 & 0.0364(36) \end{pmatrix} \mu_{\mathrm{B}}\mathrm{T}^{-1}$$

The eigenvalues of the susceptibility tensor are the diagonal values of $0.0364\mu_{\mathrm{B}}\mathrm{T}^{-1}$. The isotropic magnetization ellipsoid can be visualized in Fig. 6(f) and indicates that Cu^{2+} in $Cu(N_2D_5)_2(SO_4)_2$ has Heisenberg spins.

D. Magnetic excitations in $Cu(N_2D_5)_2(SO_4)_2$

To investigate the exchange interactions and anisotropy further, we present INS measurements on $Cu(N_2D_5)_2(SO_4)_2$. The measurements were taken at 10 K, 3 K and 0.3 K. This corresponds to the paramagnetic and long range order regions of the phase diagram shown in Fig. 5(c). The INS data is shown in Fig. 7(a)-(c). The measured low energy scattering is dominated by dispersionless features at 0.2 meV and 0.4 meV. The scattering is present at the same energy at 10 K, 3K and 0.3 K and is assigned to non-magnetic vibration modes within the material. There is, however, an apparent change in the low energy intensity underneath the vibration modes which increases in going from 10 K to 0.3 K. To explore this further Fig. 7(d)-(f) shows the temperature difference for the three temperatures collected. The remaining scattering in the temperature subtracted data has the signatures of magnetic excitations that develop as the temperature is decreased. Indeed the observation of scattering at 3 K, above the expected long range order transition of 1 K and in the nominally paramagnetic state, is expected in 1D systems that have strong interactions within the chain and reduced interactions between the chains. This will lead to low dimensional short range-ordering above T_N. In the temperature range 3 K - 10 K, shown in Fig. 7(d) there is inelastic scattering indicating correlations. This further develops in the range 0.3 K - 3 K, Fig. 7(e). We therefore consider the 0.3 K minus 10 K temperature difference data, Fig. 7(f), as best representing the inelastic magnetic signal.

To search for static short or long range order scattering we considered the elastic only scattering around E=0 meV, however, found no clear magnetic Bragg peaks or diffuse scattering. Consequently $Cu(N_2D_5)_2(SO_4)_2$ appears to be dominated by dynamic rather than static magnetic correlations.

We proceed under the assumption that the residual scattering from 10 K to 0.3 K corresponds to magnetic excitations and develop a minimal model spin

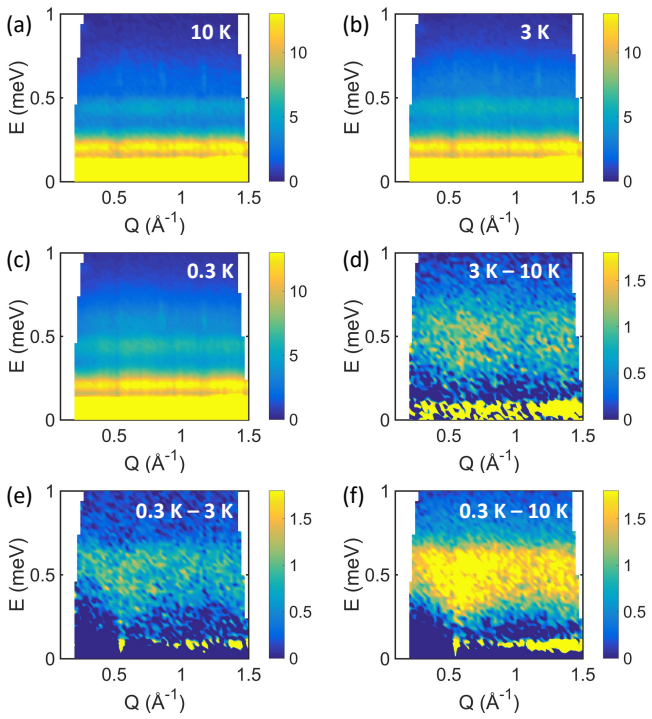

FIG. 7. Inelastic neutron scattering measurements on $Cu(N_2D_5)_2(SO_4)_2$ using the HYSPEC instrument. Measurements at (a) 10 K, (b) 3 K and (c) 0.3 K. Temperature subtracted data for (d) 3 K minus 10 K, and (e) 0.3 K minus 0.3 K and (f) 0.3 K minus 10 K.

Hamiltonian to describe the exchange interaction energy scales. We make the further approximation, based on the susceptibility data and the ordering observed in $Mn(N_2H_5)_2(SO_4)_2$, that the spins form an AFM 1D-chain with FM interactions between the chains. Alternative spin models were attempted, however did not produce good agreement with the data.

We utilize a linear-spin wave theory approach. Following the predictions of Heisenberg exchange and the results from polarized data indicating Heisenberg spins we use the Heisenberg Hamiltonian:

$$\mathcal{H} = \sum_{i,j} J_{ij}\mathbf{S}_i \cdot \mathbf{S}_j + D\sum_{i,j} S_i^2, \qquad (3)$$

where J_{ij} is the exchange interaction between neighbors i and j. D describes the single-ion anisotropy, which would provide a route for a spin-gap. As discussed below we do not find evidence for a spin-gap and all models presented have D=0 meV. Further measurements with single crystals or higher resolution techniques would be of interest to investigate any potential spin-gap.

The magnetic exchange interactions, J, considered are shown in Fig. 8(a). The nearest neighbor distance corresponding to the exchange interaction J_a is a Cu-Cu distance of 5.39 Å forming the 1D-chains along the a-axis. The next nearest neighbor distance J_b is 5.65 Å between

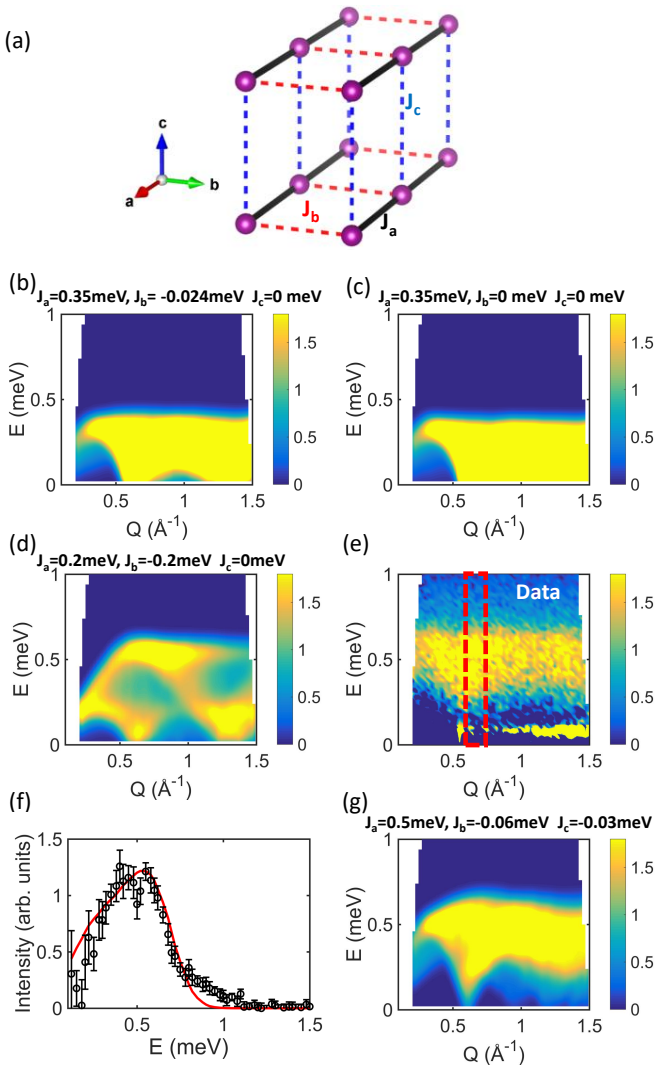

FIG. 8. (a) Exchange interactions considered in the LSWT model for the Cu ions in $Cu(N_2D_5)_2(SO_4)_2$. (b) Magnetic excitations for J_a=0.35 meV, J_b=-0.24 meV, J_c=0 meV, (c) J_a=0.35 meV, J_b=0 meV, J_c=0 meV and (d) J_a=0.2 meV, J_b=-0.2 meV, J_c=0 meV. (e) 0.3 K - 10 K data. The red dashed lines indicate a region used to perform cuts through the data during the fitting process. (f) Cut along energy with a constant Q range of 0.55 Å^{-1} to 0.65 Å^{-1}. The black circles are the data and the red line is the LSWT simulation. (g) The candidate LSWT model using exchange interactions of J_a=0.35 meV, J_b=-0.06 meV, J_c=-0.03 meV.

the chains along the b-axis, but as discussed this is expected to have weaker exchange interactions due to the indirect exchange pathways. The interaction J_c connects the chains along the c-axis and is significantly further at 7.14 Å.

The exchange interactions were previously considered theoretically and from specific heat measurements and reported as J_a= 0.35 meV and a general interchain interaction J'= 0.024 meV[12]. We use these as our starting values and utilized SpinW to test various combinations of J_a,J_b,J_c in an iterative approach.

These previously proposed theoretical values are shown in Fig. 8(b). They capture the approximate energy scales of the INS data reasonable well. For the ideal case of a 1D-chain within this model the J_b and J_c interaction values would be negligible and are set to zero. This is shown in Fig. 8(c), however it provides a poorer model than with finite J_b or J_c values, which is expected given the indications of three dimensional long-range order from heat capacity. The case for J_a=J_b, given similar Cu-Cu ion distances, is shown in Fig. 8(d). While it is possible to reproduce similar energy scales as the data, the overall model does not provide good agreement for this scenario.

To find exchange interactions values that reproduce the experimental data we took cuts through the experimental data. An example is shown in Fig. 8(e)-(f). This was a constant Q cut along energy integrated over the range 0.55-0.65 Å^{-1}. A least squares fitting procedure was used on the 1D cuts to extract the exchange interactions that best fit the data. The fitting of data against the calculated 1D cut was done outside of SpinW, with all other aspects using SpinW. Performing these cuts in addition allowed any spin-gap or need for anisotropic term to be considered. Within the statistics of the measurements no spin-gap or improvement to the model was found by including an anisotropic term. For a Cu^{2+}, S=1/2, spin-chain material no quantum spin-gap is anticipated and therefore we proceed under the assumption that any gap is negligible within the limits of the data collected.

While we cannot uniquely define the exchange values the closest agreement to the data was obtained with $J_a \gg J_b, J_c$. Fig. 7(h) shows a model simulation that captures the essential features of the data using J_a=0.5(1) meV, J_b=-0.06(3)meV and J_c=-0.03(2) meV.

We note that the agreement of the model to the data is not fully complete, with regions of S(Q,ω) that show differences in intensity. This could indicate an incomplete linear spin wave model or artifacts from the temperature subtraction. More intriguingly, however, it could be suggesting the need for a more realistic model that accounts for the underlying behavior in this material rather than the semi-classical linear spin-wave model. We considered the procedure to convert inelastic powder data into pseudo single crystal data for 1D materials, as described in Ref. 27. No spinon or other sharp features, however, were evident in this process. This may be a consequence of the data quality or indicating that the behavior departing from a 1D approximation. Further measurements, ideally on single crystals, will be of interest. Based on the INS measurements presented here $Cu(N_2D_5)_2(SO_4)_2$ is characterized by appreciable magnetic excitation intensity but no clear signal from the magnetic ground state.

IV. CONCLUSIONS

The metal hydrazinium sulfate materials $M(N_2H_5)_2(SO_4)_2$ (M=Mn, Co, Cu) have been investigated with neutron scattering measurements and thermodynamic measurements. The results reveal signatures of 1D-spin chain behavior in all materials. The dominant interactions are antiferromagnetic interactions within the chain. This was shown directly with inelastic neutron scattering on $Cu(N_2D_5)_2(SO_4)_2$ that considered the different exchange interactions.

$Mn(N_2H_5)_2(SO_4)_2$ was the only material investigated that showed long range magnetic order from neutron powder diffraction and this could be tuned with a small applied field of 2 T. This indicates the general ease to which the magnetism can be tuned in magnetic MOFs and points to promising areas of future investigations.

$Co(N_2H_5)_2(SO_4)_2$ did not yield any magnetic signal in traditional neutron powder diffraction. However, the use of PNPD was able to show several well defined peaks that were analyzed to extract the atomic site susceptibility. The results showed an anisotropic magnetization on the Co site with indications of Ising-type interactions in the *ab*-plane. All measurements on $Co(N_2H_5)_2(SO_4)_2$ were performed on non-deuterated materials and therefore the results motivate efforts towards synthesis to produce deuterated $Co(N_2H_5)_2(SO_4)_2$.

$Cu(N_2D_5)_2(SO_4)_2$ revealed no clear indications of long range magnetic order down to 0.3 K in neutron diffraction measurements. The lack of observed magnetic Bragg peaks may reasonably be explained as being due to the signal being too low to detect. The observation of a sharp anomaly in the heat capacity supports long range order. Despite the lack of any long range ordering from neutron scattering there were measurements of magnetic excitations that developed above the expected long range magnetic ordering temperature and continued to increase at lower temperatures. Consequently the dynamic rather than static magnetic correlations, in the data presented, was strongest. This may point to quantum behavior in this S=1/2 spin chain compound and motivate further measurements. A semi-classical linear spin wave model was able to reasonably well reproduce the data and yielded exchange interactions that supported the dominant intra-chain interactions.

Collectively, polarized and unpolarized neutron scattering within all materials revealed unique insights that are applicable to a wide range of related magnetic MOFs. This indicated the series $M(N_2H_5)_2(SO_4)_2$, with interchangeable M^{2+} ion and tunability is a promising model example of a well isolated 1D-spin chain within a regular crystalline lattice. Going from the S=5/2 to S=1/2 magnetic ions showed the potential to tune the system from the classical to quantum regime, pointing to interesting fundamental and applied behavior.

ACKNOWLEDGMENTS

We gratefully thank Iurri Kibalin for discussions on the polarized powder neutron data analysis. This research used resources at the High Flux Isotope Reactor and Spallation Neutron Source, a DOE Office of Science User Facility operated by the Oak Ridge National Laboratory. This research used resources at the Missouri University Research Reactor (MURR). This work was supported in part by a University of Missouri Research Council Grant (Grant Number: URC-22-021). This manuscript has been authored by UT-Battelle, LLC under Contract No. DE-AC05-00OR22725 with the U.S. Department of Energy. The United States Government retains and the publisher, by accepting the article for publication, acknowledges that the United States Government retains a non-exclusive, paidup, irrevocable, world-wide license to publish or reproduce the published form of this manuscript, or allow others to do so, for United States Government purposes. The Department of Energy will provide public access to these results of federally sponsored research in accordance with the DOE Public Access Plan(http://energy.gov/downloads/doepublic-access-plan).

* caldersa@ornl.gov

[1] P. A. Goddard, J. L. Manson, J. Singleton, I. Franke, T. Lancaster, A. J. Steele, S. J. Blundell, C. Baines, F. L. Pratt, R. D. McDonald, O. E. Ayala-Valenzuela, J. F. Corbey, H. I. Southerland, P. Sengupta, and J. A. Schlueter, Phys. Rev. Lett. **108**, 077208 (2012).
[2] G. Mnguez Espallargas and E. Coronado, Chem. Soc. Rev. **47**, 533 (2018).
[3] N. Stock and S. Biswas, Chemical Reviews **112**, 933 (2012).
[4] P. J. Saines and N. C. Bristowe, Dalton Trans. **47**, 13257 (2018).
[5] M. Kurmoo, Chem. Soc. Rev. **38**, 1353 (2009).
[6] W. Traube and W. Passarge, Berichte der deutschen chemischen Gesellschaft **46**, 1505.
[7] H. Witteveen and J. Reedijk, Solid State Communications **12**, 1121 (1973).
[8] H. Witteveen and J. Reedijk, Journal of Solid State Chemistry **10**, 151 (1974).
[9] C. Cheng, H. Wong, and W. M. Reiff, Inorganic Chemistry **16**, 819 (1977).
[10] K. Srinivasan, S. Govindarajan, and W. T. A. Harrison, Acta Crystallographica Section E **63**, i41 (2007).
[11] A. W. Parkins, P. D. Prince, R. A. L. Smith, and J. W. Steed, Acta Crystallographica Section C **57**, 670 (2001).
[12] A. Paduan-Filho, A. P. Vieira, J. G. A. Ramon, and R. S. Freitas, Journal of Physics: Condensed Matter **28**, 506004 (2016).
[13] D. W. Hand and C. K. Prout, J. Chem. Soc. A , 168 (1966).
[14] F. Klaaijsen, H. Den Adel, Z. Dokoupil, and W. Huiskamp, Physica B+C **79**, 113 (1975).
[15] V. O. Garlea, B. C. Chakoumakos, S. A. Moore, G. B. Taylor, T. Chae, R. G. Maples, R. A. Riedel, G. W. Lynn,

and D. L. Selby, Applied Physics A **99**, 531 (2010).
[16] S. Calder, K. An, R. Boehler, C. R. Dela Cruz, M. D. Frontzek, M. Guthrie, B. Haberl, A. Huq, S. A. J. Kimber, J. Liu, J. J. Molaison, J. Neuefeind, K. Page, A. M. dos Santos, K. M. Taddei, C. Tulk, and M. G. Tucker, Review of Scientific Instruments **89**, 092701 (2018).
[17] J. Rodrguez-Carvajal, Physica B: Condensed Matter **192**, 55 (1993).
[18] A. Wills, Physica B **276**, 680 (2000).
[19] J. Perez-Mato, S. Gallego, E. Tasci, L. Elcoro, G. de la Flor, and M. Aroyo, Annual Review of Materials Research **45**, 217 (2015).
[20] A. Gukasov and P. J. Brown, Journal of Physics: Condensed Matter **22**, 502201 (2010).
[21] I. A. Kibalin and A. Gukasov, Phys. Rev. Research **1**, 033100 (2019).
[22] S. Toth and B. Lake, Journal of Physics: Condensed Matter **27**, 166002 (2015).
[23] C. K. Prout and H. M. Powell, J. Chem. Soc. , 4177 (1961).
[24] W. Low, Phys. Rev. **109**, 256 (1958).
[25] F. Lloret, M. Julve, J. Cano, R. Ruiz-Garca, and E. Pardo, Inorganica Chimica Acta **361**, 3432 (2008), protagonists in Chemistry: Dante Gatteschi (Part I).
[26] B. Yuan, I. Khait, G.-J. Shu, F. C. Chou, M. B. Stone, J. P. Clancy, A. Paramekanti, and Y.-J. Kim, Phys. Rev. X **10**, 011062 (2020).
[27] K. Tomiyasu, M. Fujita, A. I. Kolesnikov, R. I. Bewley, M. J. Bull, and S. M. Bennington, Applied Physics Letters **94**, 092502 (2009).